Pérez Ruiz, R.; Molins-Molina, O.; Lence, E.; González-Bello, C.; Miranda Alonso, MÁ.; Jiménez Molero, MC. (02-1). Photogeneration of Quinone Methides as Latent Electrophiles for Lysine Targeting. The Journal of Organic Chemistry. 83(21):13019-13029. https://doi.org/10.1021/acs.joc.8b01559

JOC The Journal of Organic Chemistry

Article

Photogeneration of Quinone-Methides as Latent Electrophiles for Lysine-Targeting

Raul Perez-Ruiz, Oscar Molins-Molina, Emilio Lence, Concepción González-Bello, Miguel A Miranda, and M. Consuelo Jiménez

J. Org. Chem., **Just Accepted Manuscript** • DOI: 10.1021/acs.joc.8b01559 • Publication Date (Web): 02 Oct 2018

ACS Publications

is published by the American Chemical Society. 1155 Sixteenth Street N.W., Washington, DC 20036

Photogeneration of Quinone-Methides as Latent Electrophiles for Lysine-Targeting

Raúl Pérez-Ruiz,[a, b] Oscar Molins-Molina,[a] Emilio Lence,[c] Concepción González-Bello,[c]* Miguel A. Miranda,[a]* M. Consuelo Jiménez[a]*

[a] Departamento de Química/Instituto de Tecnología Química UPV-CSIC, Universitat Politécnica de València, Camino de Vera s/n 46071 Valencia (Spain).
[b] Photoactivated Processes Unit, IMDEA Energy Institute, Av. Ramón de la Sagra 3, 28935 Móstoles, Madrid (Spain).
[c] Centro Singular de Investigación en Química Biolóxica e Materiais Moleculares (CIQUS), Departamento de Química Orgánica, Universidade de Santiago de Compostela, Jenaro de la Fuente s/n, 15782 Santiago de Compostela (Spain).

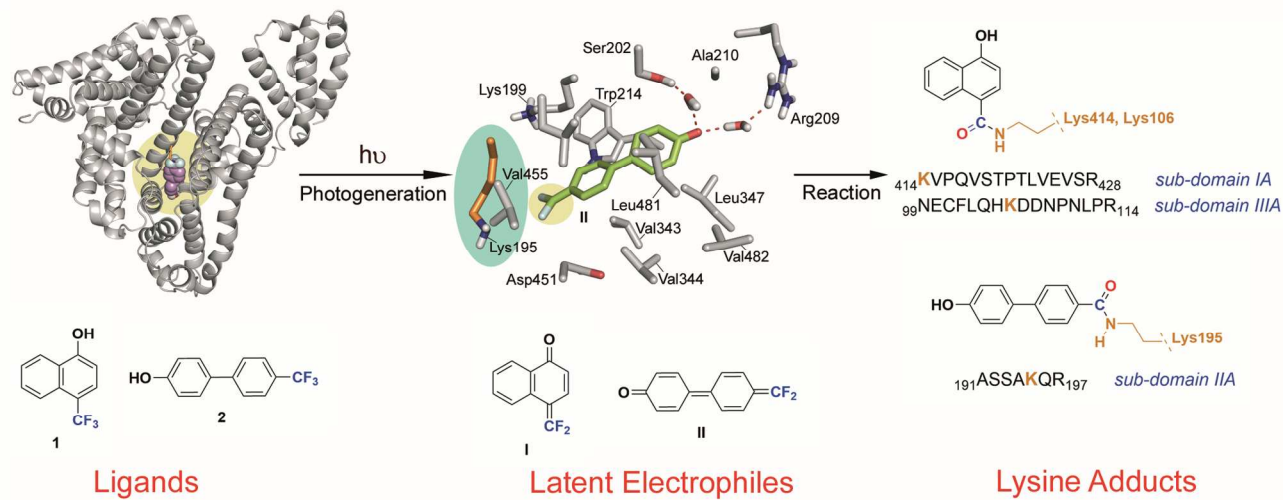

ABSTRACT: Latent electrophiles are nowadays very attractive chemical entities for drug discovery, as they are unreactive unless activated upon binding with the specific target. In this work, the utility of 4-trifluoromethyl phenols as precursors of latent electrophiles − quinone methides (QM) − for lysine-targeting is demonstrated. These Michael acceptors were photogenerated for specific covalent modification of lysine residues using human serum albumin (HSA) as a model target. The reactive QM-type intermediates **I** or **II**, generated upon irradiation of 4-trifluoromethyl-1-naphthol (**1**)@ HSA or 4-(4-trifluorometylphenyl)phenol (**2**)@HSA complexes, exhibited chemoselective reactivity towards lysine residues leading to amide adducts, which was confirmed by proteomic analysis. For ligand **1**, the covalent modification of residues Lys106 and Lys414 (located in sub-domains IA and IIIA, respectively) was observed, whereas for ligand **2**, the modification of Lys195 (in sub-domain IIA) took place. Docking and molecular dynamics simulation studies provided an insight into the molecular basis of the selectivity of **1** and **2** for these HSA sub-domains and the covalent modification mechanism. These studies open the opportunity of performing protein silencing by generating reactive ligands under very mild conditions (irradiation) for specific covalent modification of hidden lysine residues.

INTRODUCTION

Small organic molecules can undergo bioactivation *in vivo,* which affords electrophilic species able to react with biomacromolecules, leading to covalent adducts that trigger undesired toxic effects. This was already described in the 30's for the metabolites of polycyclic aromatic hydrocarbons, which were found to be highly reactive intermediates able to attach to liver proteins.[1] During the 70s, the covalent binding theory of xenobiotic-induced liver and lung toxicity emerged, as well as the idea that drug-protein adducts are potential haptens able to elicit immune-mediated adverse events. Such irreversible binding was viewed as a risk factor in drug development, either by the direct tissue damage or by the immune responses after protein haptenation. However, the last decade has witnessed the renaissance of targeted covalent inhibition in drug discovery,[2] for example in the successful treatment of cancer by covalent epidermal growth factor receptor (EGFR) inhibi-

tors.[3] The enormous advantages of irreversible drugs are associated with their high potency, low dosage, extended duration of action, selectivity and general applicability.[4] These features, together with an improved understanding of their potential risks, have resulted in a remarkable increase of the number of clinical trials, drug approvals and scientific articles in the area.[4]

In this context, binding and reactivity are the two key steps involved in "protein silencing". The former consists in the reversible association between an inhibitor (a high-affinity ligand) and its biological target, whereas the latter is the reaction between both partners to form a covalent adduct. Inhibitors of this type usually contain an electrophilic functional group that reacts with a close nucleophile on the target. Their design is highly challenging because it requires an appropriate combination of affinity, reactivity and selectivity, to avoid off-target effects. Hence, electrophiles that are unreactive unless activated upon protein binding (latent electrophiles, LEs) are of particular interest in drug development. This constitutes an attractive research field, as only few selective and safe LEs have been reported.[5]

Strategically, targeted covalent inhibition requires the catalytic action of a protein to convert a ligand into the corresponding LE within the active site (Scheme 1, pathway A). Although this is now considered as a validated tool for drug discovery, alternative strategies for addressing this issue would be desirable. One interesting possibility could be the utilization of light as an external factor to achieve direct formation of LEs from the bound ligand, without the need for any catalytic process mediated by the protein (Scheme 1, pathway B).

To inactivate proteins through formation of irreversible adducts, alkylations or Michael additions are among the most frequently employed reactions.[4c,d] Specifically, quinone methides (QMs) are good Michael acceptors that can react with the amino acid residues of proteins (commonly Cys) and other QM intermediates have been found to modify proteins;[6] in this context QM have been applied as suitable LEs for the inhibition of mammalian serine proteases and bacterial serine β-lactamases.[7] However, the photogeneration of QMs[8] within proteins has been rarely reported, despite the possibility of exciting selectively their precursors under mild conditions.[9]

Trifluoromethyl substituted aromatic moieties are present in a number of agrochemicals,[10] polymers[11] and pharmaceuticals.[12] In general, incorporation of a trifluoromethyl substituent enhances the lipophilicity of active compounds and results in a better incorporation into target cells. In comparison with other halogen-containing compounds, trifluoromethyl derivatives are less reactive[13,14] and reluctant to biological degradation[15]. However, a number of trifluoromethyl aromatics can be converted into carboxylic acid derivatives in the presence of nucleophiles upon photochemical activation.[16] In this regard, the photohydrolysis of trifluoromethyl-substituted phenols and naphthols has been previously reported to occur through formation of QM intermediates.[17]

With this background, we decided to explore the feasibility of the targeted covalent inhibition concept through photochemical generation of LEs and subsequent reaction with targeted protein nucleophiles. Compared to cysteine residues,[18] targeting nucleophilic lysine residues of the binding-sites appears more challenging and has been less exploited.[19] In this context, identification of adducts between 2-hydroxy-4-trifluoromethylbenzoic acid and the ε-amino groups of the lysine residues of ubiquitin under sunlight exposure has been recently demonstrated by photophysical and proteomic analysis.[20]

Scheme 1. Targeted Irreversible Inhibition Approaches

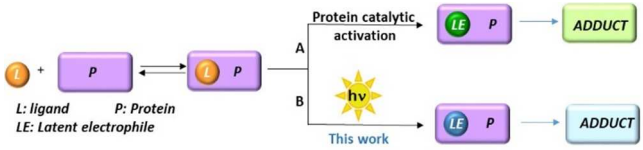

To check whether photogenerated QMs can be appropriate LEs for lysine-targeting, we selected 4-trifluoromethyl-1-naphthol (**1**) and 4-(4-trifluorometylphenyl)phenol (**2**) (Chart 1) as model compounds. The naphthalene and biphenyl chromophores should be advantageous for spectroscopic measurements. As regards the model protein, human serum albumin (HSA) was chosen taking into account its availability and dark binding capability.[21] The obtained results clearly show that formation of ground-state complexes between ligands and HSA leads ultimately to stable adducts between photogenerated LEs and lysine residues localized in the binding pockets of HSA.

Chart 1. Chemical structures of **1** and **2**

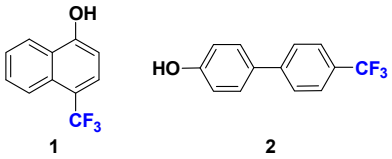

RESULTS AND DISCUSSION

The methodological approach to achieve the proposed objective involved i) characterization of the excited states of **1** and **2** in solution, both as the free compounds and in the presence of proteins, ii) proteomic studies of **1** and **2** irradiated in the presence of HSA, to detect covalent photobinding to amino acid residues and iii) theoretical calculations, to understand the binding modes and the formation of adducts. The obtained results are presented below in separated sections.

Photophysical detection of a complex between trifluoromethylphenols 1 and 2 and HSA. First, the absorption and emission properties of **1** were determined in acetonitrile and in aqueous media, under neutral and alkaline conditions (pH = 7.4 or pH=12), to ensure predominance of the phenol or the phenolate anion in the ground state. A summary of the obtained results is presented in Table 1. It was found that the free phenol absorbs at *ca*. 300 nm and emits at *ca*. 340 nm, whereas the corresponding bands of the phenolate displayed maxima at *ca*. 340 and 450 nm, respectively.

In the case of **2**, the free phenol showed absorption and emission peaking at 270-275 nm and 350-365 nm, respectively. The corresponding bands of the phenolate were found at 305 and 430 nm. Some representative spectra of **1** and **2** under different conditions are shown in Figures S1-S3 of the Supporting Information.

Table 1. Photophysical properties of **1** and **2**

Compound	Medium	$(\lambda_{max})_{abs}$/nm	$(\lambda_{max})_{em}$/nm
1	MeCN	295	342
	pH = 7.4	301	446
	pH = 12	343	447
	HSA	327,373	420
2	MeCN	275	348
	pH = 7.4	270	364
	pH = 12	306	430
	HSA	315	415

When the absorption spectrum of **1** was recorded in PBS, in the presence of HSA, a new band emerged above 320 nm, which increased with increasing concentrations of protein. A similar trend was observed for **2** in the presence of HSA, although the new band was more intense compared to that of **1** (Figures S4A,B). In both cases, the new bands were attributed to a ground-state complex with HSA. Selective excitation of the complexes led to new emission bands centered at λ = 420 nm (**1**) or λ = 415 nm (**2**), which again increased with increasing concentrations of protein (Figure S4C,D) and were different from those previously ascribed to the corresponding phenol or phenolate (Figure 1A,B); they were attributed to emission from the above mentioned HSA complexes. Control experiments, consisting on excitation of HSA alone, indicated the absence of emission arising from the protein under the experimental conditions (Figure S5). The stoichiometry of the **1**@HSA and **2**@HSA complexes was determined as 2:1 and 1:1, respectively, by means of Job plot analysis (SI, Figure S6).[22] To evidence formation of **1**@HSA and **2**@HSA complexes, difference spectra, i. e. [**1**@HSA]-[**1**+HSA], were obtained upon variations of ligand/protein molar ratios (Figures S7A and S8A). To calculate the binding constants, the Benesi-Hildebrand procedure[23] (eq. 1, Figures S7B and S8B) was employed.

$$\frac{[Ligand]}{Abs_{complex}} = \frac{1}{K_{complex} \times [HSA] \times \varepsilon_{complex}} + \frac{1}{\varepsilon_{complex}} \qquad \text{Eq. 1°}$$

where $Abs_{complex}$ is the maximum absorbance of complexes (at 373 nm for **1** and 315 nm for **2**) at different HSA concentrations and $\varepsilon_{complex}$ is the molar absorption coefficient. The hhg-affinity $K_{complex}$ values, determined from the slope, are 2.4×10^5 M^{-1} and 2.8×10^4 M^{-1}, for **1** and **2**, respectively. These results are consistent with data previously reported for similar compounds such as naphthol and hydroxybiphenyl.[24]

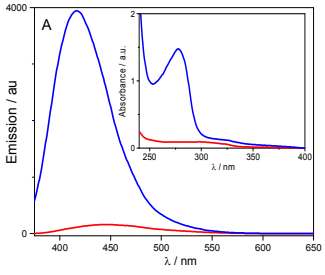

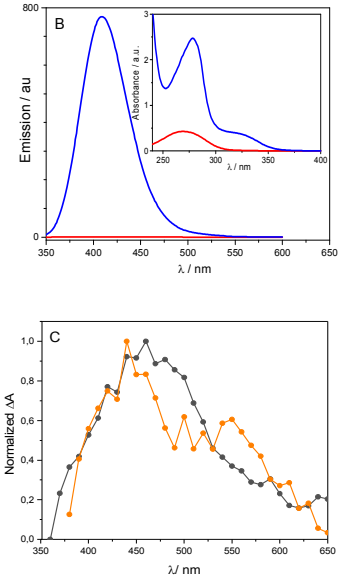

Figure 1. Emission (large) and absorption (inset) spectra, recorded in PBS (red) and in the presence of 2 equivalents of HSA (blue) for **1** (A) and **2** (B), respectively; λ_{exc} was 355 nm for **1** and 324 nm for **2**. (C): Normalized transient absorption spectra obtained for **1** (orange) and **2** (black) in PBS in the presence of 5 equivalents of HSA, upon laser excitation at 355 nm. In all measurements, [**1**] = 0.05 mM, [**2**] = 0.05 mM

Laser flash photolysis of the **1**@HSA and **2**@HSA complexes was also performed upon excitation at 355 nm. In both cases, the resulting transient absorption spectra (Figure 1C) were tentatively ascribed to the expected quinone methides **I** and **II** (Chart II), based on the existing data on related compounds. Their lifetimes were 0.5 and 8.0 μs, respectively.[8h,i]

Photobinding of 1 and 2 to HSA. Irradiation of **1** and **2** in aqueous media (λ_{max} = 300 nm) led to the corresponding carboxylic acids, in agreement with the previously reported result for similar substrates. The accepted mechanism involves deprotonation in the singlet excited state, followed by heterolytic C-F bond cleavage to afford a QM-type intermediate (**I** or **II**, Chart 2).[17]

Photolysis of **1**@HSA and **2**@HSA was performed for detecting the possible formation of covalent photoadducts ([ligand] = 5×10^{-5}M; ligand:protein 1:5 molar ratio, air/PBS, $\lambda_{max\ irr.}$ = 300 nm). The photodegradation process was monitored by fluorescence spectroscopy (Figure S9). Then, trypsin digestion (to cleave peptide chains mainly at the carboxyl side of Lys or Arg residues, unless there is a neighboring Pro residue) was run, coupled with HPLC-MS/MS analysis. Full-scan and fragmentation data files were treated by using the MascotS database search engine, in order to find out which (if any) of the Lys residues located inside the hydrophobic binding sites of the protein became covalently modified by nucleophilic trapping of intermediates **I** or **II** (Chart 2).

Chart 2. Chemical structures of the QM intermediates **I** and **II** together with the Lys trapping products

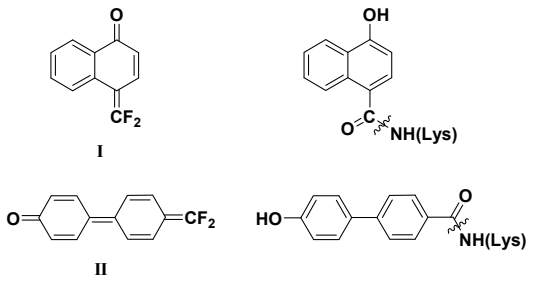

In the case of **1**, an increment of *ca*. 170 amu was observed in peptides $_{99}$**NECFLQHKDDNPNLPR**$_{114}$ (Mr exp. = 2165.9548, Mr calc. 2165.9589) and $_{414}$**KVPQVSTPTLVEVSR**$_{428}$ (Mr exp. = 1808.9629, Mr calc. = 1808.9673). The MS/MS analysis revealed modification of Lys106 (in subdomain IA). The MS/MS fragment ions showed an unmodified y ion series from y_2 to y_8, whereas an increment of m/z 298 amu was detected at Lys106 between y_8 and y_9 corresponding to $C_{11}H_7O_2$–Lys(–H_2O). Besides, Lys414 (in sub-domain IIIA) was also modified, with a Lys106:Lys 414 ratio of *ca*. 85. A suggested reaction mechanism is outlined in Scheme 2. A similar analysis for **2** showed an increment of 196 amu in $_{191}$**ASSAKQR**$_{197}$ (Mr exp = 942.4536, Mr calc. = 942.4559) with covalent binding at Lys195 (located in sub-domain IIA). In this case, the MS/MS fragment ions showed an unmodified y ion series from y_3 to y_6, while an increment of m/z 324 amu was detected at Lys195 between y_2 and y_3 corresponding to $C_{13}H_9O_2$–Lys(–H_2O). Details of the ESI-MS/MS spectra and fragmentation patterns are shown in Figures S10-S13 in the SI.

Scheme 2. Proposed covalent modification mechanism for **1**.

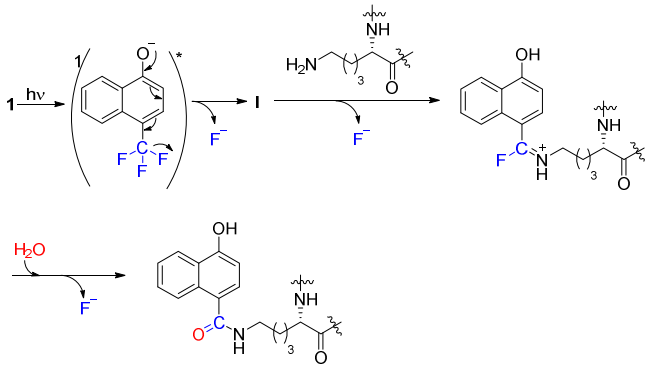

Docking and Molecular Dynamics Simulations Studies. In an effort to understand in atomic detail the covalent modification mechanism as well as to gain insight into the molecular basis of the

observed selectivities, docking and Molecular Dynamics (MD) simulation studies were carried out.

*Binding of **1** to HSA and covalent addition to sub-domains IA and IIIA*- The binding modes of ligand **1** in sub-domains IA and IIIA of HSA were first studied by molecular docking using the program GOLD[25] version 5.2 and the available protein coordinates of the crystallographically determined HSA in complex with iophenoxic acid (PDB code 2YDF).[26] This structure was chosen because two of the four molecules observed are located close to Lys414. The positions of these molecules in sub-domain IIIA and of the ε-amino group of Lys106 in sub-domain IA were used to define the recognition site, and the radius was set to 8 Å. The highest score solutions obtained by docking were further analyzed by MD simulation studies in order to assess the stability and therefore the reliability of the postulated binding. The monomer of the **1**@HSA-IA and **1**@HSA-IIIA protein complexes in a truncated octahedron of water molecules obtained with the molecular mechanics force field AMBER[27] was employed. The binding mode of the intermediate **I** was also studied by manual replacement of the ligand **1** with **I** in the binary **1**@HSA-IA and **1**@HSA-IIIA complexes, which was then subjected to 60 ns of dynamic simulation. Moreover, as for compound **1** the experimentally observed stoichiometry ligand *vs* HSA was 2:1, the ternary **1**+**1**@HSA complex was also considered. These studies revealed sub-domain IA as the main binding pocket of **1**, which will be discussed below.

(a) *Binary **1**@HSA-IA complex.* The results from the dynamic simulation of the **1**@HSA-IA complex showed that the proposed binding for **1** in sub-domain IA obtained by docking was reliable as this complex proved to be very stable (Figure 2). Analysis of the root-mean-square deviation (rmsd) for the whole protein backbone (C_α, C, N and O atoms) calculated in the complex obtained from MD simulations studies revealed that it varies between 1.0–3.0 Å (average of 1.6 Å) and is relatively low for sub-domain IA (0.9–1.3 Å and an average of 0.9 Å) (Figure S14). Ligand **1** would be anchored to sub-domain IA of HSA *via* two hydrogen bonding interactions involving the phenol group and the main carbonyl group of Tyr148 and the amide side chain of Gln196 (Figures 2A and 2B). Analysis of the variation of the relative distance between the atoms involved in the aforementioned hydrogen bonding interactions during the whole simulation revealed that **1** is well fixed in this pocket and its conformation properly controlled by these residues (Figure 2C). The CF_3 moiety would be also located in the proximity of ε-amino group of Lys106 with an average distance of 5.3 Å during the simulation. In addition, ligand **1** would stablish numerous apolar interactions within the pocket, mainly involving the side chain of residues Leu103, Ala151, Leu250, Gly248, Cys246, Cys200 and the carbon side chain of Gln29.

(b) *Binary **I**@HSA-IA complex.* As it is shown in Figure 2D, the results of our computational studies revealed that the intermediate **I** would be anchored to sub-domain IA of HSA *via* hydrogen bonding interaction with the main NH group of Ala151. The analysis of the relative distance between the C19 atom (CF_2 group) in **I** and the NZ atom of Lys106 and O17 atom (carbonyl group) in **I** and NH group of Ala151 during the simulation revealed that this contact is present during 92% of the simulation with an average distance of 3.0 Å (Figure 2E). Furthermore, the difluoromethide moiety in **I** would be located closer to the ε-amino group of Lys106 (average distance of 4.8 Å) than in the **1**@HSA-IA complex (Figures 2C *vs* 2E). This proposed arrangement of the intermediate **I** adequately explains the experimentally observed modification of Lys106.

Once the intermediate **I** is generated by irradiation of the **1**@HSA protein complex, covalent attachment would probably occur by nucleophilic attack of Lys106, which would be triggered by Asp108 acting as the general base and through the generation of the tyrosinate form of Tyr148 (Figure 2D). Thus, during 90% of the simulation a water molecule from the

bulk solvent remained fixed between the side chain of Asp108 and Tyr148, with one of its protons engaged in a hydrogen bond with a carboxylate oxygen of Asp108 and one of its oxygen's lone pairs accepting a hydrogen bond from the oxygen atom of Tyr148. Under this arrangement, the tyrosinate could be generated and be the general base for the deprotonation of Lys106 (nucleophile). The average distance between the NZ atom of Lys106 and the O atom of Tyr148, the O atom of Tyr148 and the O atom of the water molecule and the closest OD1/OD2 atoms (carboxyl group) of Asp108 and the O atom of the water molecule during the whole simulation is 5.50 Å, 2.85 Å and 2.73 Å, respectively (Figure S15). The generation of catalytic tyrosinates in proteins by neighbor aspartate residues, either involving or not a water molecule, has previously been reported.[28]

(c) *Binary* ***1****@HSA-IIIA complex.* In general, the computational studies carried out with the binary complex **1**@HSA-IIIA reveal that in contrast to the binary complex **1**@HSA-IA in which the CF_3 group of the ligand is located close to the lysine that is modified, Lys106, the latter group would be placed further away from Lys414 (Figure 3). In particular, the average distance between the NZ atom of Lys414 and the C19 atom (CF_3 group) is of 9.0 Å during the 60 ns of simulation (Figure 3C, brown line). Moreover, the ligand would be located in this pocket due to a strong hydrogen bonding with the main carbonyl group of Leu430 (average distance of 5.6 Å, Figure 3C, yellow line) as well as diverse apolar interactions with the side chain of residues Leu407, Val433, Leu453, Ala449, Ile388, Leu387 and Phe403, and the carbon chain of Asn391 (Figure 3B). Remarkably, the overall binding stability of ligand **1** in sub-domain IIIA seems to be lower than in sub-domain IA in view of the greater mobility of the ligand in the pocket. This is because the binding pocket of the sub-domain IA is smaller and the polar interactions with the protein are stronger. These findings also revealed that the primary binding pocket of ligand **1** would be sub-domain IA. In this case, residue Glu492, which is located close by Lys414, would act as the general base for the deprotonation of the lysine residue that undergoes covalent modification. The average distance between the NZ atom of Lys414 and the closest OE1/OE2 atoms (carboxylate grou) of Glu492 is 4.66 Å during the whole simulation (Figure S16).

(d) *Ternary* ***1+1****@HSA complex*. The experimentally observed 2:1 complex was also studied (Figure 3D). In general, no significant differences were observed in the binding of **1** to sub-domain IA in the ternary and binary complexes, locating in both cases the CF_3 group of **1** in close contact to the ε-amino group of Lys106 (average distance of 5.1 Å *vs* 5.3 Å, respectively) (Figures 3E *vs* 2C, black lines). More importantly, the presence of **1** in this pocket would significantly reduce the distance between the ε-amino group of Lys414 and the CF_3 group in **1** for covalent modification. These findings also reveal that: (1) sub-domain IA would be the primary binding pocket of **1**, and (2) this last binding would have a positive cooperative effect that would favor the binding to sub-domain IIIA.

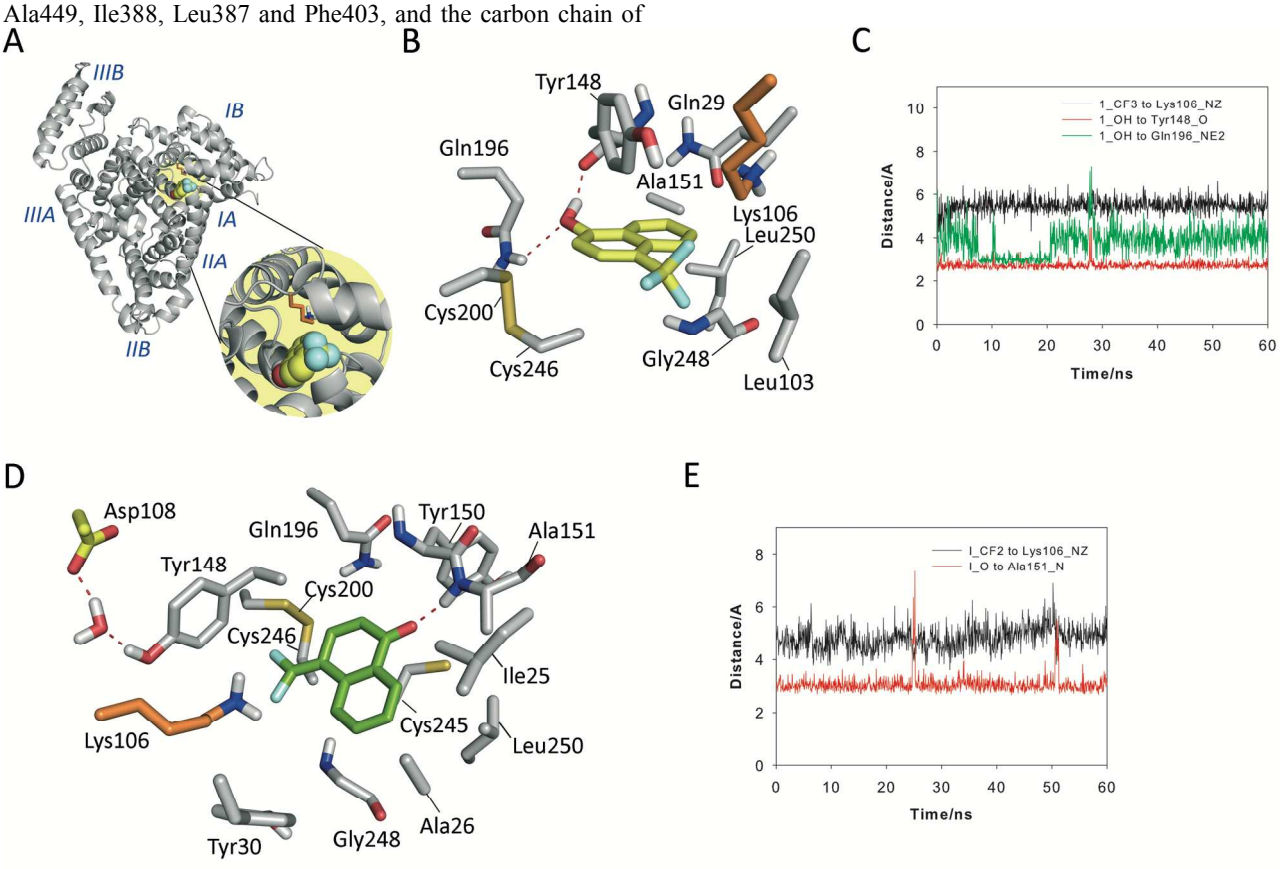

Figure 2. Proposed binding mode of **1** (yellow) and the intermediate **I** (green) in sub-domain IA as obtained by MD simulation studies. (A) Overall view of the proposed binary **1**@HSA-IA complex. Snapshot after 60 ns is shown. (B) Detailed view of the **1@**HSA-IA complex. (C) Variation of the relative distance between the C19 (CF_3 group) and the O atom of **1** and the NZ atom of

Lys106, the O atom of Tyr148 and the NE2 atom of Gln196, respectively, in the **1**@HSA-IA protein complex during 60 ns of simulation. (D) Detailed view of the binary **I**@HSA-IA complex. Snapshot after 30 ns is shown. (E) Variation of the relative distance between the C19 (CF_2 group) in **I** and the NZ atom of Lys106 and O17 atom (carbonyl group) in **I** and NH group of Ala151 in the **I**@HSA-IA protein complex during the whole simulation. Relevant side chain residues are shown and labelled. Lys106 and Asp108 are shown in orange and yellow, respectively. Hydrogen bonding interactions are shown as red dashed lines. Note how for both complexes the lysine residue that is covalently modified (Lys106) is located very close to the fluoromethide moiety and the phenol group in **1** and the ketone group in **I** would be anchored in the pocket by strong hydrogen bonding interactions.

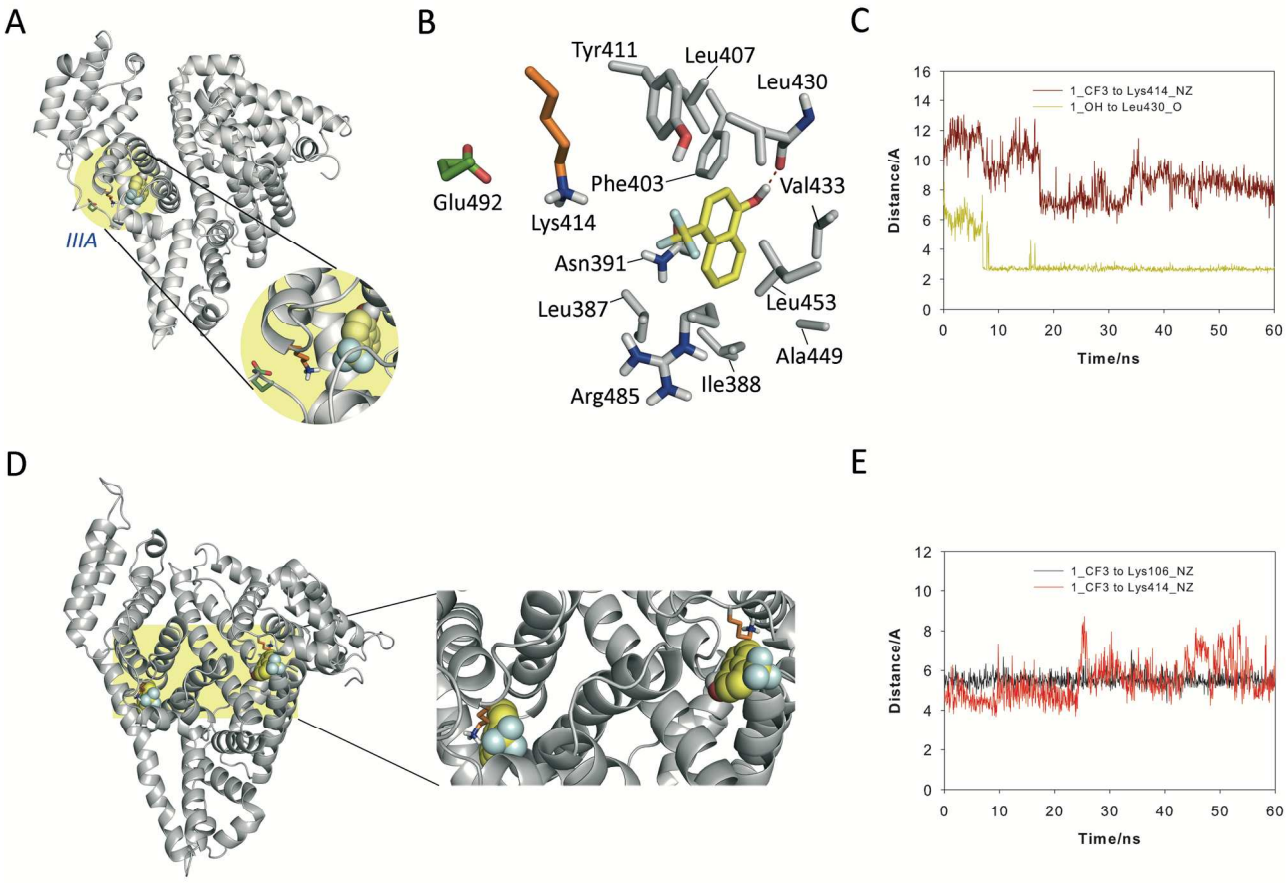

Figure 3. Proposed binding mode of **1** in binary **1**@HSA-IIIA and ternary **1**+**1**@HSA complexes as obtained by MD simulation studies. (A) Overall view of the proposed binary **1**@HSA-IIIA complex. Snapshot after 50 ns is shown. (B) Detailed view of the **1**@HSA-IIIA complex. (C) Variation of the relative distance between the C19 (CF_3 group) and O atom of **1** and the NZ atom of Lys414 and the O atom of Leu430, respectively, in the **1**@HSA-IIIA protein complex during 60 ns of simulation. (D) Overall view of the proposed ternary **1**+**1**@HSA complex. Snapshot after 20 ns is shown. (E) Variation of the relative distance between the C19 (CF_3 group) of **1** and the NZ atom of Lys106 and Lys414 in the **1**@HSA-IIIA and **1**+**1**@HSA complexes, respectively, during 60 ns of simulation. Relevant side chain residues are shown and labelled. Lys414 and Glu492 are shown in orange and yellow, respectively. Hydrogen bonding interactions are shown as red dashed lines. Note how Lys414 is located closer to the CF_3 group in **1** in the ternary **1**+**1**@HSA complex than in the binary one.

The analysis of the rmsd for the whole protein backbone (C_α, C, N and O atoms) and the sub-domains IA and IIIA calculated in the ternary **1**+**1**@HSA complex also corroborate the increased stability of these protein pockets (Figure S9D). The computational results explain the abovementioned photophysical and proteomic experimental results. Moreover, the MD simulation studies carried out with the corresponding ternary adducts revealed that the intermediate **I** would be rapidly trapped, in particular by Lys414 as its mobility in this pocket is very significant.

*Binding of **2** to HSA and covalent addition to sub-domain IIA* – As for ligand **1**, the binding mode of ligand **2** in sub-domain IIA of HSA was first studied by molecular docking using the protein coordinates found in the crystal structure of HSA in complex with oxyphenbutazone (PDB code 2BXB[29]). The ligand in this structure is located close to the experimentally observed modified Lys195 residue. It is important to highlight that an analysis of the residues surrounding Lys195 revealed that this residue is located nearby another lysine residue, Lys199, whose modification was not observed (Figure 4). Considering that when two lysine residues are located very close in space, usually only one of them is protonated at physiological pH, simulation studies with the two possible protonation states of both lysine residues were performed. The best

results were obtained considering neutral Lys195 (nucleophile) and protonated Lys199, which would be also in agreement with the experimental results. Furthermore, although the obtained binding mode reveals that both residues are close in distance to the CF3 group in **2**, the arrangement of the side chain of Lys199 observed during 60 ns of simulation revealed to be geometrically inappropriate for nucleophilic attack once the intermediate **II** would be generated (Figures 4B and 4D). The ε-amino group in Lys199 is predicted to be parallel to the ligand during the whole simulation rather than facing to the difluoromethide group in **II** for chemical modification. The binary **2**@HSA-IIA complex probed to be very stable, confirming the reliability of the proposed binding (Figure S17). Unlike ligand **1**, direct polar contacts between ligand **2** and the residues

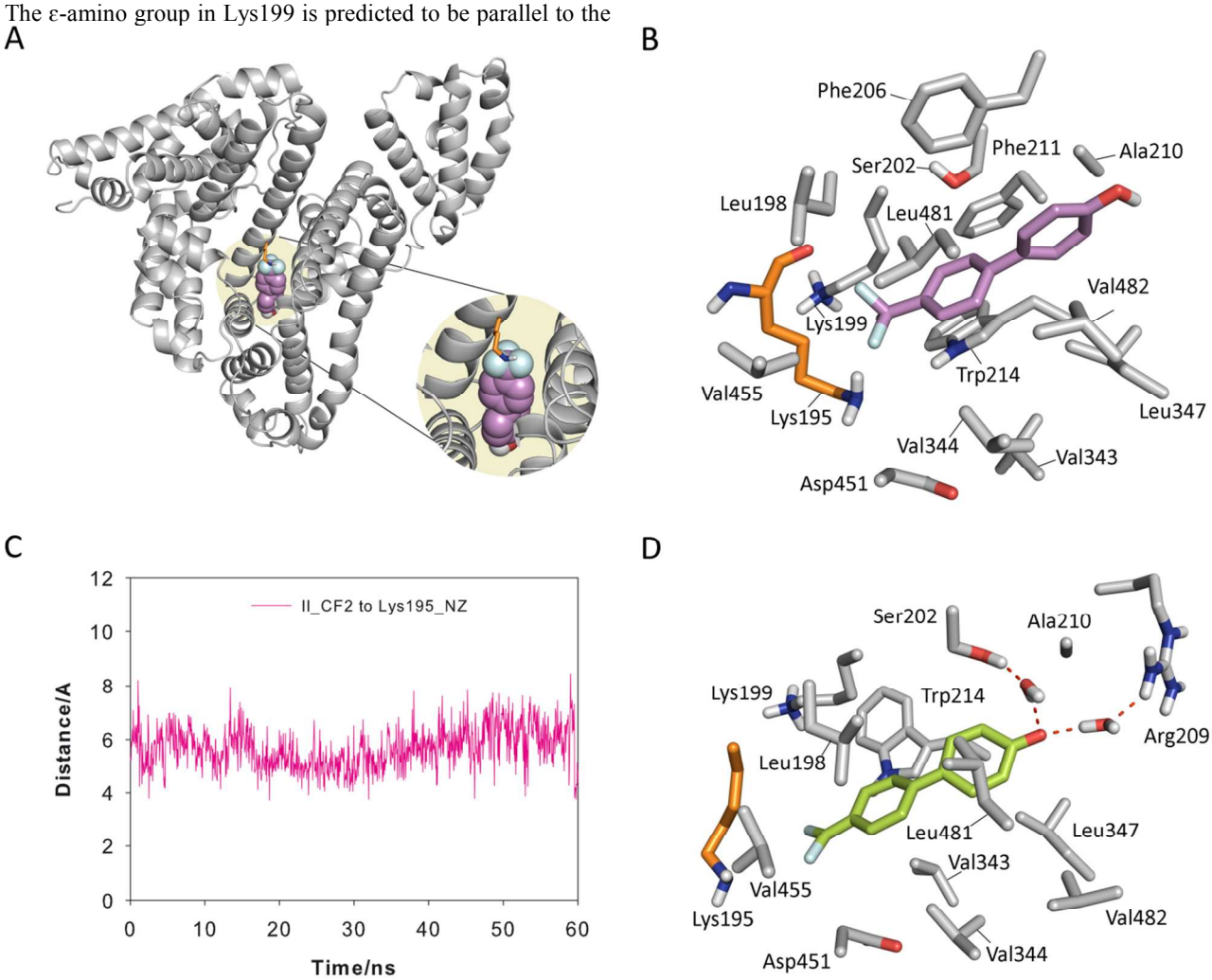

Figure 4. Proposed binding mode of the ligand **2** (violet) and the intermediate **II** (green) in sub-domain IIA as obtained by MD simulation studies. (A) Overall view of the proposed binary **2**@HSA-IIA complex. Snapshot after 60 ns is shown. (B) Detailed view of the binary **2**@HSA-IIA complex. (C) Variation of the relative distance between the C23 atom (CF_2 group) and the NZ atom of Lys195 in the **II**@HSA-IIA protein complex during 60 ns of simulation. (D) Detailed view of the **II**@HSA-IIA adduct. Snapshot after 20 ns is shown. Note how Lys195 is well located for nucleophilic attack. Relevant side chain residues are shown and labelled. Hydrogen bonding interactions of the intermediate **II** are shown as red dashed lines.

within the pocket were not identified. In this case, the polar interactions of the phenol moiety in **2**, which fixes this ligand in the pocket, would be mediated by water molecules (not shown). Moreover, ligand **2** would be embedded in a large apolar pocket involving residues Val343, Val344, Val482, Leu347, Leu481, Val455, Leu198, Phe206, Phe211, Ala210, Trp214 and the carbon side chain of Asp451 and Ser202.

The intermediate **II** generated by irradiation of the **2**@HSA-IIA protein complex would have a similar binding mode as ligand **2** (Figure 4D). As for **2**, no direct polar contacts between **II** and the protein were observed. Instead, the ketone group in **II** would interact with the side chain of Ser202 and Arg209 through water molecules. Under this arrangement, the ε-amino group of Lys195 is well located for nucleophilic attack to the difluoromethide moiety in **II**. Thus, the analysis of the variation of the relative distance between the C23 atom (CF_2 group) and the NZ atom of Lys195 in the **II**@HSA-IIA protein adduct during 60 ns of simulation revealed an average distance of 5.7 Å (Figure 4C).

CONCLUSIONS

The combined experimental and theoretical results suggest that quinone methides photogenerated from trifluoromethylphenols can be appropriate latent electrophiles to achieve selective lysine targeting. Thus, **1** and **2** form ground-state complexes with HSA, characterized by a long-wavelength absorption band with maxima at *ca*. 320 nm, which allows their selective excitation, resulting in a well-defined emission appearing at *ca*. 420 nm. Photolysis of the complexes produces a covalently modified protein, whose proteomic analysis reveals selective targeting of Lys 106 and, to a lesser extent, Lys 414, in the case of ligand **1**; by contrast, Lys 195 becomes selectively modified upon irradiation of ligand **2** within HSA. The results of our MD simulation studies revealed that not only the ligands but also the photogenerated intermediates form stable complexes with the identified pockets of HSA, which would explain the selective modification of the internal lysine residues, Lys106, Lys414, and Lys195. The computational studies performed with the binary **1**@HSA-IA and **1**@HSA-IIIA and ternary **1**+**1**@HSA complexes reveal sub-domain IA as the main binding pocket of **1**. Ligand **1** would be anchored to this pocket *via* two hydrogen bonding interactions involving the phenol group and the main carbonyl group of Tyr148 and the amide side chain of Gln19. After irradiation, the photogenerated intermediate **I** would be fixed to this pocket *via* hydrogen bonding interaction with the main NH group of Ala151 allowing the difluoromethide moiety in **I** to be located close to the ε-amino group of Lys106 for nucleophilic attack. In addition, binding to sub-domain IA would have a positive cooperative effect that would favor the binding to sub-domain IIIA. This is in agreement with the experimentally observed modification of Lys106 and Lys414 residues in a ratio of *ca*. 85:1, respectively. On the other hand, the intermediate **II** photogenerated from ligand **2** would bind to sub-domain IIA *via* polar contacts with the side chain of Ser202 and Arg209 mediated by water molecules. Under this arrangement, the ε-amino group of Lys195 would be well located for nucleophilic attack to the difluoromethide moiety in **II**.

EXPERIMENTAL SECTION

General. Human serum albumin and 4'-hydroxy-4-biphenylcarboxylic acid were commercially available. Spectrophotometric, HPLC or reagent grade solvents were used without further purification. Buffered saline solutions at pH 7.4 and pH 12 were prepared by dissolving commercially available tablets in deionized water. Ligands 4-trifluoromethyl-1-naphthol (**1**) and 4-(4-trifluorometylphenyl)phenol (**2**), were synthesized following previously reported procedures.[30]

Absorption and emission measurements. Optical spectra at different media were recorded on a JASCO V-630 spectrophotometer. Steady-state emission and excitation spectra were recorded on a JASCO FP-8500 spectrofluorometer system, provided with a monochromator in the wavelength range of 200-850 nm, at 22°C. Time-resolved fluorescence measurements were performed with an EasyLife V spectrometer from OBB (Palaiseau, France), equipped with a pulsed LED (λ_{exc} 295 nm) as excitation source. The kinetic traces were fitted by one monoexponential decay function, using a deconvolution procedure to separate them from the lamp pulse profile. Experiments were performed on solutions of known concentration in different media, employing 10 × 10 mm^2 quartz cells with 4 mL capacity.

Laser flash photolysis measurements. Experiments were carried out with a pulsed Nd:YAG Laser system with 355 nm as excitation wavelength, 0.6 cm as beam diameter and a pulse duration of 10 ns. The energy was set at 15 mJ/pulse. The apparatus consisted of the pulsed laser, a xenon lamp, a monochromator, and a photomultiplier. Samples of **1** and **2** in the presence of 5 equivalents of HSA were placed in 10 mm × 10 mm quartz cells. The absorbance of the complexes at the excitation wavelength was kept at 0.25. Experiments were performed at 22°C.

Steady-state photolysis experiments. Irradiations of **1** or **2** (5×10^{-5} M) were performed in PBS in the presence or absence of HSA (ligand/protein 1:5 molar ratio) in a multilamp photoreactor containing low pressure mercury lamps (14 × 8 W), with emission maximum at λ= 300 nm, through Pyrex. The course of the process was followed by monitoring the changes in the fluorescence spectra of the reaction mixtures at increasing times.

Protein Digestion and LC-ESI-MS/MS Analysis. Human serum albumin (HSA) was enzymatically digested into smaller peptides using trypsin. Subsequently, these peptides were analyzed using nanoscale liquid chromatography coupled to tandem mass spectrometry (nano LC-MS/MS). Briefly, 20 µg of sample were taken (according to Qubit quantitation) and the volume was set to 20 µL. Digestion was achieved with sequencing grade trypsin (Promega) according to the following steps: i) 2 mM DTT in 50 mM NH_4HCO_3 V = 25 µL, 20 min (60 °C); ii) 5.5 mM IAM in 50 mM NH_4HCO_3 V=30 µL, 30 min (dark); iii) 10 mM DTT in 50 mM NH_4HCO_3 V = 60 µL, 30 min; iv) Trypsin (Trypsin: Protein ratio 1:20 w/w) V = 64 µL, overnight 37 °C. Digestion was stopped with 7 µL 10% TFA (Cf protein *ca* 0.28 µg/µL). Next, 5 µL of sample (except the main bands) were loaded onto a trap column (NanoLC Column, 3µ C18-CL, 350 um × 0.5 mm; Eksigent) and desalted with 0.1% TFA at 3 µL/min during 5 min. The peptides were then loaded onto an analytical column (LC Column, 3 µ C18-CL, 75 um × 12 cm, Nikkyo) equilibrated in 5% acetonitrile 0.1% formic acid. Elution was carried out with a linear gradient of 5 to 45% B in A for 30 min (A: 0.1% formic acid; B: acetonitrile, 0.1% formic acid) at a flow rate of 300 µL/min. Peptides were analyzed in a mass spectrometer nanoESI qQTOF (5600 TripleTOF, ABSCIEX). The tripleTOF was operated in information-dependent acquisition mode, in which a 0.25-s TOF MS scan from 350–1250 m/z was performed, followed by 0.05-s product ion scans from 100-1500 m/z on the 50 most intense 2-5 charged ions. ProteinPilot v4.5. (ABSciex) search engine default parameters were used to generate peak list directly from 5600 TripleTOF wiff files. The obtained mgf was used for identification with MASCOT (v 4.0, Matrix- Science). Database search was performed on SwissProt database. Searches were done with tryptic specificity allowing one missed cleavage and a tolerance on the mass measurement of 100 ppm in MS mode and 0.6 Da in MS/MS mode.

Docking studies. They were carried out using program GOLD 5.2.2[23] and the protein coordinates found in the crystal structure of HSA in complex with: (a) oxyphenbutazone (PDB code 2BXB[29]) for **2** and iophenoxic acid (PDB code 2YDF[24]) for **1**. These structures were selected since the observed lig-

ands are located in the same region where the lysine residues covalently modified by **1** and **2** were observed. Ligand geometries were minimized using the AM1 Hamiltonian as implemented in the program Gaussian 09[31] and used as MOL2 files. Each ligand was docked in 25 independent genetic algorithm (GA) runs, and for each of these a maximum number of 100000 GA operations were performed on a single population of 50 individuals. Operator weights for crossover, mutation and migration in the entry box were used as default parameters (95, 95, and 10, respectively), as well as the hydrogen bonding (4.0 Å) and van der Waals (2.5 Å) parameters. The position of the side chain of the experimentally observed modified residue was used to define the active-site and the radius was set to 8 Å. All crystallographic water molecules and the ligands were removed for docking. The "flip ring corners" flag was switched on, while all the other flags were off. The GOLD scoring function was used to rank the ligands in order to fitness.

Molecular dynamic simulations. *(a) Ligand minimization*. The ligand geometries of the highest score solution obtained by docking were minimized using a restricted Hartree–Fock (RHF) method and a 6–31G(d) basis set, as implemented in the ab initio program Gaussian 09. Partial charges were derived by quantum mechanical calculations using Gaussian 09, as implemented in the R.E.D. Server (version 3.0),[32] according to the RESP[33] model. Ligand coordinates obtained by docking were employed as starting point for MD simulations. The missing bonded and non-bonded parameters were assigned, by analogy or through interpolation, from those already present in the AMBER[34] database (GAFF[35]).

(b) Generation and minimization of the complexes. Simulations of the HSA/**2** and HSA/**1** binary complexes were carried out using the enzyme geometries in PDB codes 2BXB and 2YDF, respectively. Computation of the protonation state of titratable groups at pH 7.0 was carried out using the H^{++} Web server.[36] Addition of hydrogen and molecular mechanics parameters from the ff14SB[37] and GAFF force fields, respectively, were assigned to the protein and the ligands using the LEaP module of AMBER Tools 15.[29] As a result of this analysis: (i) His535 was protonated in δ position; (ii) His3, His9, His39, His146, His242, His288, His440, His464 and His510 were protonated in ε position; (iii) His67, His105, His128, His247, His338 and His367 were protonated in δ and ε positions. The protein was immersed in a truncated octahedron of ~25000 TIP3P water molecules and neutralized by addition of sodium ions. The system was minimized in five stages: (a) minimization of poorly unsolved residues: (i) for PDB 2BXB: 12, 33, 41, 51, 56, 60, 73, 81, 82, 84, 94, 95, 97, 111, 114, 174, 186, 190, 205, 209, 225, 227, 240, 250, 275, 276, 277, 297, 301, 313, 317, 321, 359, 390, 402, 436, 439, 444, 466, 513, 519, 524, 532, 536, 538, 541, 545, 550, 551, 560, 562, 564, 565, 574 and 580; and (ii) for PDB 2YDF: 12, 16, 31, 33, 41, 48, 56, 60, 64, 69, 77, 81, 82, 84, 93, 94, 95, 97, 98, 104, 109, 114, 115, 119, 121, 132, 136, 137, 141, 159, 160, 162, 167, 174, 178, 186, 190, 195, 205, 262, 269, 276, 277, 280, 301, 302, 305, 313, 314, 317, 351, 359, 365, 372, 376, 389, 390, 397, 402, 425 ,432, 436, 439, 444, 459, 466, 500, 502, 503, 505, 507, 509, 510, 512, 513, 516, 520, 524, 525, 536, 541, 543, 545, 548, 549, 550, 551, 554, 560, 562, 563, 564, 565, 568, 570, 571, 573, 574, 575, 580 and 582 (1000 steps, first half using steepest descent and the rest using conjugate gradient); (b) minimization of the ligand (1000 steps, first half using steepest descent and the rest using conjugate gradient); (c) minimization of the solvent and ions (5000 steps, first half using steepest descent and the rest using conjugate gradient); (d) minimization of the side chain residues, waters and ions (5000 steps, first half using steepest descent and the rest using conjugate gradient); (e) final minimization of the whole system (5000 steps, first half using steepest descent and the rest using conjugate gradient). A positional restraint force of 50 kcal mol^{-1} $Å^{-2}$ was applied to not minimized residues of the protein during the stages a-c and to α carbons during the stage d, respectively.

(c) Simulations. MD simulations were performed using the pmemd.cuda_SPFP[38-40] module from the AMBER 14 suite of programs. Periodic boundary conditions were applied and electrostatic interactions were treated using the smooth particle mesh Ewald method (PME)[41] with a grid spacing of 1 Å. The cutoff distance for the non-bonded interactions was 9 Å. The SHAKE algorithm[42] was applied to all bonds containing hydrogen using a tolerance of 10^{-5} Å and an integration step of 2.0 fs. The minimized system was then heated at 300 K at 1 atm by increasing the temperature from 0 K to 300 K over 100 ps and by keeping the system at 300 K another 100 ps. A positional restraint force of 50 kcal mol^{-1} $Å^{-2}$ was applied to all α carbons during the heating stage. Finally, an equilibration of the system at constant volume (200 ps with positional restraints of 5 kcal mol^{-1} $Å^{-2}$ to α alpha carbons) and constant pressure (another 100 ps with positional restraints of 5 kcal mol^{-1} $Å^{-2}$ to α alpha carbons) were performed. The positional restraints were gradually reduced from 5 to 1 mol^{-1} $Å^{-2}$ (5 steps, 100 ps each), and the resulting systems were allowed to equilibrate further (100 ps). Unrestrained MD simulations were carried out for 100 ns. System coordinates were collected every 10 ps for further analysis. The molecular graphics program PyMOL[43] was employed for visualization and depicting ligand/protein structures. The cpptraj module in AMBER 14 was used to analyse the trajectories and to calculate the root-mean-square deviations (rmsd) of the protein during the simulation.[44]

ASSOCIATED CONTENT

Supporting Information: Experimental procedures for the synthesis and characterization of compound **1**–**2**, docking and MD simulation studies. Extra figures of the phothophysical studies (Figures S1-S9), proteomic analysis (Figures S10-S13), MD simulation studies (Figures S14−S17). "The cartesian coordinates of all the complexes included in this work are also provided." This material is available free of charge via the Internet at http://pubs.acs.org.

AUTHOR INFORMATION

Corresponding Authors

*mcjimene@qim.upv.es;
*mmiranda@qim.upv.es;
*concepcion.gonzalez.bello@usc.es

ORCID

Raúl Pérez-Ruiz: 0000-0003-1136-3598

Emilio Lence: 0000-0001-9489-9421

Concepción González-Bello: 0000-0001-6439-553X

Miguel A. Miranda: 0000-0002-7717-8750

M. Consuelo Jiménez: 0000-0002-8057-4316

ACKNOWLEDGMENTS

Financial support from the Spanish Ministry of Economy and Competiveness [CTQ2016-78875-P, SAF2016-75638-R and BES□2014□069404 (pre-doctoral fellowship to O. M.-M.)], the Generalitat Valenciana (PROMETEO/2017/075), the Community of Madrid (2016-T1/AMB-1275), the Xunta de Galicia (Centro Singular de Investigación de Galicia accreditation 2016−2019, ED431G/09 and post-doctoral fellowship to E. L.) and the European Union (European Regional Development Fund − ERDF) is gratefully acknowledged. The proteomic analysis was performed in the proteomics facility of SCSIE University of Valencia that belongs to ProteoRed PRB2-ISCIII and is supported by grant PT13/0001, of the PE I+D+i 2013–2016, funded by ISCIII and FEDER.

REFERENCES

(1) (a) Evans, D. C.; Watt, A. P.; Nicoll-Griffith, D. A.; Baillie, T. A. Drug-Protein Adducts: An Industry Perspective on Minimizing the Potential for Drug Bioactivation in Drug Discovery and Development. *Chem. Res. Toxicol* **2004**, *17*, 3−16. (b) Reid, W. D.; Krishna, G.; Gillette, J. R.; Brodie B. B. Biochemical Mechanism of Hepatic Necrosis Induced By Aromatic Hydrocarbons. *Pharmacology* **1973**, *10*, 193−214.

(2) (a) Singh, J.; Petter, R. C.; Baillie, T. A.; Whitty, A. The Resurgence of Covalent Drugs. *Nat. Rev. Drug Discov.* **2011**, *10*, 307−317. (b) Baillie, T. A. Targeted Covalent Inhibitors for Drug Design. *Angew. Chem. Int. Ed.* **2016**, *55*, 13408−13421.

(3) Wang, S.; Cang, S.; Liu, D. Third-Generation Inhibitors Targeting EGFR T790M Mutation In Advanced Non-Small Cell Lung Cancer. *J. Hematol. Oncol.* **2016**, *9*, 34/1−34/7.

(4) (a) Smith, A. J. T.; Zhang, X.; Leach, A. G.; Houk, K. N. Beyond Picomolar Affinities: Quantitative Aspects of Noncovalent and Covalent Binding of Drugs to Proteins. *J. Med. Chem.* **2009**, *52*, 225−233. (b) Potashman, M. H.; Duggan, M. E. Covalent Modifiers: an Orthogonal Approach to Drug Design. *J. Med. Chem.* **2009**, *52*, 1231−1246. (c) Noe, M. C.; Gilbert, A. M. Targeted Covalent Enzyme Inhibitors. *Annu. Rep. Med. Chem.* **2012**, *47*, 413−439. (d) Lanning, B. R.; Whitby, L. R.; Dix, M. M.; Douhan, J.; Gilbert, A. M.; Hett, E. C.; Johnson, T. O.; Joslyn, C.; Kath, J. C.; Niessen, S.; Roberts, L. R.; Schnute, M. E.; Wang, C.; Hulce, J. J.; Wei, B.; Whiteley, L. O.; Hayward, M. M.; Cravatt, B. J. A Road Map to Evaluate the Proteome-Wide Selectivity of Covalent Kinase Inhibitors. *Nat. Chem. Biol.* **2014**, *10*, 760−767. (e) González-Bello, C. Designing Irreversible Inhibitors--Worth the Effort?. *ChemMedChem* **2016**, *11*, 22−30.

(5) (a) Katzenellenbogen, J. A.; Carlson, K. E.; Heiman, D. F.; Robertson, D. W.; Wei, L. L.; Katzenellenbogen, B. S. Efficient and Highly Selective Covalent Labeling of the Estrogen Receptor with [3H]Tamoxifen Aziridine. *J. Biol. Chem.* **1983**, *258*, 3487−3495. (b) Staub, I.; Sieber, S. A. Beta-Lactams as Selective Chemical Probes for the in vivo Labeling of Bacterial Enzymes Involved in Cell Wall Biosynthesis, Antibiotic Resistance, and Virulence. *J. Am. Chem. Soc.* **2008**, *130*, 13400−13409. (c) Ekkebus, R.; van Kasteren, S. I.; Kulathu, Y.; Scholten, A.; Berlin, I.; Geurink, P. P.; de Jong, A.; Goerdayal, S.; Neefjes, J.; Heck, A. J. R.; Komander, D.; Ovaa, H. On Terminal Alkynes that Can React with Active-Site Cysteine Nucleophiles in Proteases. *J. Am. Chem. Soc.* **2013**, *135*, 2867−2870. (d) Liu, Q.; Sabnis, Y.; Zhao, Z.; Zhang, T.; Buhrlage, S. J.; Jones, L. H.; Gray, N. S. Developing Irreversible Inhibitors of the Protein Kinase Cysteinome. *Chem. Biol.* **2013**, *20*, 146−159. (e) Shannon, D. A.; Banerjee, R.; Webster, E. R.; Bak, D. W.; Wang, C.; Weerapana, E. Investigating the Proteome Reactivity and Selectivity of Aryl Halides. *J. Am. Chem. Soc.* **2014**, *136*, 3330−3333. (f) Shannon, D. A.; Weerapana, E. Covalent Protein Modification: the Current Landscape of Residue-specific Electrophiles. *Curr. Opin. Chem. Biol.* **2015**, *24*, 18−26. (g) Mortenson, D. E.; Brighty, G. J.; Plate, L.; Bare, G.; Chen, W.; Li, S.; Wang, H.; Cravatt, B. F.; Forli, S.; Powers, E. T.; Sharpless, K. B.; Wilson, I. A.; Kelly, J. W. "Inverse Drug Discovery" Strategy to Identify Proteins that are Targeted by Latent Electrophiles as Exemplified by Aryl Fluorosulfates. *J. Am. Chem. Soc.* **2018**, *140*, 200−210.

(6) (a) Freccero, M. Quinone Methides as Alkylating and Cross-Linking Agents. *Mini-Reviews Org. Chem.* **2004**, *1*, 403–415. (b) Wang, P.; Song, Y.; Zhang, L.; He, H.; Zhou, X. Quinone Methide Derivatives: Important Intermediates to DNA Alkylating and DNA Cross-Linking Actions. *Curr. Med. Chem.* **2005**, *12*, 2893–2913. (c) Van De Water, R. W.; Pettus, T. R. R. O-Quinones Methides: Intermediates Underdeveloped and Underutilized in Organic Synthesis. *Tetrahedron* **2002**, *58*, 5367–5405. (d) McCracken, P. G.; Bolton, J. L.; Thatcher, G. R. J. Covalent Modification of Proteins and Peptides by the Quinone Methide from 2-*tert*-Butyl-4,6-dimethylphenol: Selectivity and Reactivity with Respect to Competitive Hydration. *J. Org. Chem.* **1997**, *62*, 1820−1825. (e) Bolton, J. L.; Turnipseed, S. B.; Thompson, J. A. *Chem. Biol. Interact.* **1997**, *107*, 185−200.

(7) Rokita, S. E. Quinone Methides; John Wiley & Sons, Inc.: Hoboken, New Jersey (2009), chapter 11, pp 357−383.

(8) (a) Basarić, N.; Mlinarić-Majerski, K.; Kralj, M. Quinone Methides: Photochemical Generation and its Application in Biomedicine. *Curr. Org. Chem.* **2014**, *18*, 3−18. (b) Škalamera, D.; Mlinarić-Majerski, K.; Kleiner, I. M.; Kralj, M.; Oake, J.; Wan, P; Bohne, C; Basarić, N. Photochemical Formation of Anthracene Quinone Methide Derivatives. *J. Org. Chem*. **2017**, *82*, 6006−6021. (c) Doria, F.; Lena, A.; Bargiggia, R.; Freccero, M. Conjugation, Substituent, and Solvent Effects on the Photogeneration of Quinone Methides. *J. Org. Chem.* **2016**, *81*, 3665−3673. (d) Husak, A.; Noichl, B. P.; Ramljak, T. S.; Sohora, M.; Škalamera, D.; Budišab, N.; Basarić, N. Photochemical Formation of Quinone Methides From Peptides Containing Modified Tyrosine. *Org. Biomol. Chem.* **2016**, *14*, 10894−10905. (e) Škalamera, D.; Bohne, C.; Landgraf, S., Basarić, N. Photodeamination Reaction Mechanism in Aminomethyl p-Cresol Derivatives: Different Reactivity of Amines and Ammonium Salts. *J. Org. Chem*. **2015**, *80*, 10817−10828. (f) Percivalle, C.; La Rosa, A.; Verga, D.; Doria, F.; Mella, M.; Palumbo, M.; Di Antonio, M.; Freccero, M. Quinone Methide Generation via Photoinduced Electron Transfer. *J. Org. Chem.* **2011**, *76*, 3096−3106. (g) Modica, E.; Zanaletti, R.; Freccero, M.; Mella, M. Alkylation of Amino Acids and Glutathione in Water by *O*-Quinone Methide. Reactivity and Selectivity. *J. Org. Chem*. **2001**, *66*, 41−52. (h) Shi, Y; Wan, P. Charge Polarization in Photoexcited Alkoxy-Substituted Biphenyls: Formation of Biphenyl Quinone Methides. *Chem. Commun*. **1995**, 1217−1218. (i) Basaric, N.; Cindro, N.; Bobinac, D.; Mlinaric-Majerski, K.; Uzelac, L.; Kraljb, M., Wan, P. Sterically Congested Quinone Methides in Photodehydration Reactions of 4-Hydroxybiphenyl Derivatives and Investigation of Their Antiproliferative Activity. *Photochem. Photobiol. Sci*. **2011**, *10*, 1910−1921.

(9) (a) Jiang, J.; Zeng, D.; Li, S. Photogenerated Quinone Methides as Protein Affinity Labeling Reagents. *ChemBioChem* **2009**, *10*, 635−638. (b) Arumugam, S.; Guo, J.; Mbua, N. E.; Friscourt, F.; Lin, N.; Nekongo, E.; Boons, G.-J.; Popik V. V. Selective and Reversible Photochemical Derivatization of Cysteine Residues in Peptides and Proteins. *Chem. Sci.* **2014**, *5*, 1591−1598.

(10) (a) Tingle, C. C.; Rother, J. A.; Dewhurst, C. F.; Lauer, S.; King, W. J. Fipronil: Environmental Fate, Ecotoxicology, and Human Health Concerns. *Rev. Environ. Contam. Toxicol.* **2003**, *176*, 1−66. (b) Nizamani, S. M.; Hollingworth, R. M. Fentrifanil: A Diarylamine Acaricide with Potent Mitochondrial Uncoupling Activity. *Biochem. Biophys. Res. Commun.* **1980**, *96*, 704−710.

(11) Huff, J. Does Exposure to Bisphenol A Represent a Human Health Risk?**.** *Regul. Toxicol. Pharmacol.* **2003**, *37*, 407−408.

(12) Wong, D. T.; Bymaster, F. P.; Engleman, E. A. Prozac (Fluoxetine, Lilly 110140), The First Selective Serotonin Uptake Inhibitor and An Antidepressant Drug: Twenty Years Since its First Publication**.** *Life Sci.* **1995**, *57*, 411−441.

(13) Quistad, G. B.; Mulholland, K. M. Metabolism of P-Chlorobenzotrifluoride by Rats. *J. Agric. Food Chem.* **1983**, *31*, 585−589.

(14) Kobayashi, Y.; Kumadaki, I. Reactions of Aromatic Trifluoromethyl Compounds with Nucleophilic Reagents. *Acc. Chem. Res.* **1978**, *11*, 197−204.

(15) Engesser, H.; Cain, R. B.; Knackmuss, H. J. Bacterial Metabolism of Side Chain Fluorinated Aromatics: Cometabolism of 3-Trifluoromethyl(TFM)-Benzoate by *Pseudomonas putida* (Arvilla) mt-2 and *Rhodococcus rubropertinctus* N657. *Arch. Microbiol.* **1988**, *149*, 188−197.

(16) (a) Caffieri, S.; Miolo, G.; Seraglia, R.; Dalzoppo, D.; Toma, F. M.; van Henegouwen, G. M. Photoaddition of Fluphenazine to Nucleophiles in Peptides and Proteins. Possible Cause of Immune Side Effects. *Chem. Res. Toxicol.* **2007**, *20*, 1470−1476. (b) Lam, M. W.; Young, C. J.; Mabury, S. A. Aqueous Photochemical Reaction Kinetics and Transformations of Fluoxetine. *Environ. Sci. Technol.* **2005**, *39*, 513−522. (c) Chaignon, P.; Cortial, S.; Guerineau, V.; Adeline, M.-Th.; Giannotti, C.; Fan, G.; Ouazzani, J. Photochemical Reactivity of Trifluoromethyl Aromatic Amines: The Example of 3,5-Diamino-Trifluoromethyl-Benzene (3,5-DABTF). *Photochem. Photobiol.* **2005**, *81*, 1539−1543. (d) Boscá, F.; Cuquerella, M. C.; Marín, M. L.; Miranda, M. A. Photochemistry of 2-Hydroxy-4-Trifluoromethylbenzoic Acid, Major Metabolite of The Photosensitizing Platelet Antiaggregant Drug Triflusal. *Photochem. Photobiol.* **2001**, *73*, 463−468. (e) Montanaro, S.; Lhiaubet-Vallet, V.; Jiménez, M. C.; Blanca, M.; Miranda, M. A. Photonucleophilic Addition of the Epsilon-Amino Group of Lysine to a Triflusal Metabolite as a Mechanistic Key to Photoallergy Mediated by the Parent Drug. *ChemMedChem.* **2009**, *4*, 1196−1202.

(17) (a) Seiler, P.; Wirz, J. The Photohydrolysis of Eight Isomeric Trifluoromethylnaphthols. *Tetrahedron Lett.* **1971**, *20*, 1683−1686. (b) Seiler, P.; Wirz, J. Struktur Und Photochemische Reaktivität: Photohydrolyse von Trifluormethylsubstituierten Phenolen und Naphtholen. *Helv. Chim. Acta* **1972**, *55*, 2693−2712. (c) Horspool, W.; Lenci, F. Handbook of Organic Chemistry and Photobiology 2nd Ed; CRC Press: Boca Raton (2004), Chapter 39, pp. 12.

(18) (a) Wu, S. J.; Luo, H.; Wang, H. N.; Zhao, W. J.; Hu, Q. W.; Yang, Y. L. Cysteinome: The First Comprehensive Database for Proteins with Targetable Cysteine and Their Covalent Inhibitors. *Biochem. Biophys. Res. Commun.* **2016**, *478*, 1268–1273. (b) Jöst, C.; Nitsche, C.; Scholz, T.; Roux, L.; Klein, C. D. Promiscuity and Selectivity in Covalent Enzyme Inhibition: A Systematic Study of Electrophilic Fragments**.** *J. Med. Chem.* **2014**, *57*, 7590–7599. (c) Marino, S. M.; Gladyshev, V. N. *J. Mol. Biol.* **2010**, *404*, 902–916. (d) Wissner, A.; Overbeek, E.; Reich, M. F.; Floyd, M. B.; Johnson, B. D.; Mamuya, N.; Rosfjord, E. C.; Discafani, C.; Davis, R.; Shi, X. Q.; Rabindran, S. K.; Gruber, B. C.; Ye, F.; Hallett, W. A.; Nilakantan, R.; Shen, R.; Wang, Y. F.; Greenberger, L. M.; Tsou, H. R. Synthesis and Structure−Activity Relationships of 6,7-Disubstituted 4-Anilinoquinoline-3-carbonitriles. The Design of an Orally Active, Irreversible Inhibitor of the Tyrosine Kinase Activity of the Epidermal Growth Factor Receptor (EGFR) and the Human Epidermal Growth Factor Receptor-2 (HER-2). *J. Med. Chem.* **2003**, *46*, 49–63. (e) Knight, J. D.; Qian, B.; Baker, D.; Kothary, R. Conservation, Variability and the Modeling of Active Protein Kinases. *PLoS One* **2007**, *2*, e982.

(19) Pettinger, J.; Jones, K.; Cheeseman, M. D. Lysine-targeting Covalent Inhibitors. *Angew. Chem. Int. Ed.* **2017**, *56*, 15200−15209.

(20) Nuin, E.; Pérez-Sala, D.; Lhiaubet-Vallet, V.; Andreu, I.; Miranda, M. A. Photosensitivity to Triflusal: Formation of a Photoadduct with Ubiquitin Demonstrated by Photophysical and Proteomic Techniques. *Front. Pharmacol.* **2016**, *7*, 277/1−277/8.

(21) (a) Peters, T. Serum Albumin. *Adv. Prot. Chem*. **1985**, 37, 161–245. (b) Raghhansen, U. Molecular Aspects of Ligand Binding to Serum Albumin. *Pharmacol. Rev.* **1981**, *33*, 17–53. (c) Vayá, I.; Lhiaubet-Vallet, V.; Jiménez, M. C.; Miranda, M. A. Photoactive Assemblies of Organic Compounds and Biomolecules: Drug-Protein Supramolecular Systems. *Chem. Soc. Rev.* **2014**, *43*, 4102−4122.

(22) (a) Huang, C. Y. Determination of Binding Stoichiometry by The Continuous Variation Method: The Job Plot. *Methods Enzymol.* **1982**, *87*, 509-525. (b) Job, P. Formation and Stability of Inorganic Complexes in Solution. *Ann. Chim.* **1928**, *9*, 113−203.

(23) Benesi, H. G.; Hildebrand, J. H. A Spectrophotometric Investigation of the Interaction of Iodine with Aromatic Hydrocarbons. *J. Am. Chem. Soc.* **1949**, *71*, 2703−2707.

(24) (a) Ahmad, E.; Rabbani, G.; Zaidi, N.; Singh, S.; Rehan, M.; Khan, M. M.; Rahman, S. K.; Quadri, Z.; Shadab, M.; Ashraf M. T.; Subbarao, N. Stereo-Selectivity of Human Serum Albumin to Enantiomeric and Isoelectronic Pollutants Dissected by Spectroscopy, Calorimetry and Bioinformatics. *PLoS One,* **2011**, *6*, e26186. (b) Mao, H.; Hajduk, P. J.; Craig, R.; Bell, R.; Borre, T.; Fesik, S. W. Rational Design of Diflunisal Analogues with Reduced Affinity for Human Serum Albumin. *J. Am. Chem. Soc*. **2001**, *123*, 10429−10435. (c) Aureli, L.; Cruciani, G.; Cesta, M. C.; Anacardio, R.; De Simone, L.; Moriconi, A. Predicting Human Serum Albumin Affinity of Interleukin-8 (CXCL8) Inhibitors by 3D-QSPR Approach**.** *J. Med. Chem.* **2005**, *48*, 2469−2479.

(25) http://www.ccdc.cam.ac.uk/solutions/csd-discovery/components/gold/

(26) Ryan, A. J.; Chung, C. W.; Curry, S. Crystallographic Analysis Reveals The Structural Basis of The High-Affinity Binding of Iophenoxic Acid to Human Serum Albumin. *BMC Struct. Biol.* **2011**, *11*, 18.

(27) Case, D. A.; Berryman, J. T.; Betz, R. M.; Cerutti, D. S.; Cheatham III, T. E.; Darden, T. A.; Duke, R. E.; Giese, T. J.; Gohlke, H.; Goetz, A. W.; Homeyer, N.; Izadi, S.; Janowski, P.; Kaus, J.; Kovalenko, A.; Lee, T. S.; LeGrand, S.; Li, P.; Luchko, T.; Luo, R.; Madej, B.; Merz, K. M.; Monard, G.; Needham, P.; Nguyen, H.; Nguyen, H. T.; Omelyan, I.; Onufriev, A.; Roe, D. R.; Roitberg, A.; Salomon-Ferrer, R.; Simmerling, C. L.; Smith, W.; Swails, J.; Walker, R. C.; Wang, J.; Wolf, R. M.; Wu, X.; York, D. M.; Kollman, P. A. AMBER 2015, University of California, San Francisco, **2015**.

(28) (a) Coderch, C.; Lence, E.; Peón, A.; Lamb, H.; Hawkins, A. R.; Gago, F.; González-Bello, C. Mechanistic Insight Into The Reaction Catalysed by Bacterial Type II Dehydroquinases**.** *Biochem. J.* **2014**, *458*, 547−557. (b) Lence, E.; van der Kamp, M. W.; González-Bello, C.; Mulholland, A. J. QM/MM Simulations Identify The Determinants of Catalytic Activity Differences Between Type II Dehydroquinase Enzymes. *Org. Biomol. Chem.* **2018**, *16*, 4443−4455.

(29) Ghuman, J.; Zunszain, P. A.; Petitpas, I.; Bhattacharya, A. A.; Otagiri, M.; Curry, S. Structural Basis of The Drug-Binding Specificity of Human Serum Albumin. *J. Mol. Biol.* **2005**, *353*, 38–52.

(30) (a) Stahly, G. P.; Bell, D. R. A New Method for Synthesis of Trifluoromethyl-Substituted Phenols and Anilines. *J. Org. Chem.* **1989**, *54*, 2873−2877. (b) Parrish, C. A.; Adams, N. D.; Auger, K. R.; Burgess, J. L.; Carson, J. D.; Chaudhari, A. M.; Copeland, R. A.; Diamond, M. A.; Donatelli, C. A.; Duffy, K. J.; Faucette, L. F.; Finer, J. T.; Huffman, W. F.; Hugger, E. D.; Jackson, J. R.; Knight, S. D.; Luo, L.; Moore, M. L.; Newlander, K. A.; Ridgers, L. H.; Sakowicz, R.; Shaw, A. N.; Sung, C. M.; Sutton, D.; Wood, K. W.; Zhang, S. Y.; Zimmerman, M. N.; Dhanak, D. Novel ATP-Competitive Kinesin Spindle Protein Inhibitors. *J. Med. Chem.* **2007**, *50*, 4939−4952.

(31) Frisch, M. J.; Trucks, G. W.; Schlegel, H. B.; Scuseria, G. E.; Robb, M. A.; Cheeseman, J. R.; Scalmani, G.; Barone, V.; Mennucci, B.; Petersson, G. A.; Nakatsuji, H.; Caricato, M.; Li, X.; Hratchian, H. P.; Izmaylov, A. F.; Bloino, J.; Zheng, G.; Sonnenberg, J. L.; Hada, M.; Ehara, M.; Toyota, K.; Fukuda, R.; Hasegawa, J.; Ishida, M.; Nakajima, T.; Honda, Y.; Kitao, O.; Nakai, H.; Vreven, T.; Montgomery, Jr. J. A.; Peralta, J. E.; Ogliaro, F.; Bearpark, M.; Heyd, J. J.; Brothers, E.; Kudin, K. N.; Staroverov, V. N.; Kobayashi, R.; Normand, J.; Raghavachari, K.; Rendell, A.; Burant, J. C.; Iyengar, S. S.; Tomasi, J.; Cossi, M.; Rega, N.; Millam, J. M.; Klene, M.; Knox, J. E.; Cross, J. B.; Bakken, V.; Adamo, C.; Jaramillo, J.; Gomperts, R.; Stratmann, R. E.; Yazyev, O.; Austin, A. J.; Cammi, R.; Pomelli, C.; Ochterski, J. W.; Martin, R. L.; Morokuma, K.; Zakrzewski, V. G.; Voth, G. A.; Salvador, P.; Dannenberg, J. J.; Dapprich, S.; Daniels, A. D.; Farkas, Ö.; Foresman, J. B.; Ortiz, J. V.; Cioslowski, J.; Fox, D. J. Revision D.01, Gaussian, Inc., Wallingford CT, **2009**.

(32) (a) Vanquelef, E.; Simon, S.; Marquant, G.; Garcia, E.; Klimerak, G.; Delepine, J. C.; Cieplak, P.; Dupradeau, F.-Y. R.E.D. Server: A Web Service for Deriving RESP and ESP Charges and Building Force Field Libraries for New Molecules and Molecular Fragment. *Nucleic Acids Res.* **2011**, *39*, W511−W517. (b) http://upjv.q4md-forcefieldtools.org/RED/ (accessed December 1, 2017). (c) Dupradeau, F.-Y.; Pigache, A.; Zaffran, T.; Savineau, C.; Lelong, R.; Grivel, N.; Lelong, D.; Rosanski, W.; Cieplak, P. The R.E.D. Tools: Advances in RESP and ESP Charge Derivation and Force Field Library Building. *Phys. Chem. Chem. Phys.* **2010**, *12*, 7821−7839.

(33) Cornell, W. D.; Cieplak, P.; Bayly, C. I.; Gould, I. R.; Merz, K. M.; Ferguson, D. M.; Spellmeyer, D. C.; Fox, T.; Caldwell, J. W.; Kollman, P. A. A Second Generation Force Field for the Simulation of Proteins, Nucleic Acids, and Organic Molecules. *J. Am. Chem. Soc.* **1995**, *117*, 5179−5197.

(34) Case, D. A.; Cheatham, T. E.; Darden, T.; Gohlke, H., Luo, R.; Merz, K. M.; Onufriev, O.; Simmerling, C.; Wang, B.; Woods, R. J. The Amber Biomolecular Simulation Programs. *J. Comput. Chem.* **2005**, *26*, 1668–1688.

(35) (a) Wang, J.; Wolf, R. M.; Caldwell, J. W.; Kollman, P. A.; Case, D. A. Development and Testing of a General Amber Force Field**.** *J. Comp. Chem.* **2004**, *25*, 1157−1174. (b) Wang, J.; Wang, W.; Kollman, P. A.; Case, D. A. Automatic Atom Type and Bond Type Perception in Molecular Mechanical Calculations. *J. Mol. Graphics Modell.* **2006**, *25*, 247–260.

(36) (a) Gordon, J. C.; Myers, J. B.; Folta, T.; Shoja, V.; Heath, L. S.; Onufriev, A. H++: A Server for Estimating pKas and Adding Missing Hydrogens to Macromolecules. *Nucleic Acids Res.* **2005**, *33* (Web Server issue):W368. (b) http://biophysics.cs.vt.edu/H++.

(37) Maier, J. A.; Martinez, C.; Kasavajhala, K.; Wickstrom, L.; Hauser, K. E.; Simmerling, C. Ff14sb: Improving the Accuracy of Protein Side Chain and Backbone Parameters from Ff99sb. *J. Chem. Theory Comput.* **2015**, *11*, 3696–3713.

(38) Goetz, A. W.; Williamson, M. J.; Xu, D.; Poole, D.; Le Grand, S.; Walker, R. C. Routine Microsecond Molecular Dynamics Simulations with AMBER on GPUs. 1. Generalized Born. *J. Chem. Theory Comput.* **2012**, *8*, 1542−1555.

(39) Salomon-Ferrer, R.; Goetz, A. W.; Poole, D.; Le Grand, S.; Walker, R. C. Routine Microsecond Molecular Dynamics Simulations with AMBER on GPUs. 2. Explicit Solvent Particle Mesh Ewald. *J. Chem. Theory Comput.* **2013**, *9*, 3878−3888.

(40) Le Grand, S.; Goetz, A. W.; Walker, R. C. SPFP: Speed Without Compromise−A Mixed Precision Model For GPU Accelerated Molecular Dynamics Simulations. *Comp. Phys. Comm.* **2013**, *184*, 374−380.

(41) Darden, T. A.; York, D.; Pedersen, L. G. Particle Mesh Ewald: An Nlog(N) Method For Ewald Sums In Large Systems. *J. Chem. Phys.* **1993**, *98*, 10089−10092.

(42) Ryckaert, J.-P.; Ciccotti, G.; Berendsen, H. J. C. Numerical Integration of the Cartesian Equations of Motion of a System with Constraints: Molecular Dynamics of *n*-Alkanes. *J. Comput. Phys.* **1977**, *23*, 327–341.

(43) DeLano, W. L. The PyMOL Molecular Graphics System. (2008) DeLano Scientific LLC, Palo Alto, CA, USA. http://www.pymol.org/

(44) Roe, D. R.; Cheatham, T. E. PTRAJ and CPPTRAJ: Software for Processing and Analysis of Molecular Dynamics Trajectory Data. *J. Chem. Theory Comput.* **2013**, *9*, 3084–3095.